The mechanical behaviour of SentryGlas® ionomer and TSSA silicon bulk materials at different temperatures and strain rates under uniaxial tensile stress state

Santarsiero, Manuel; Louter, Christian; Nussbaumer, Alain

DOI
10.1007/s40940-016-0018-1

Publication date
2016

Document Version
Final published version

Published in
Glass Structures and Engineering

Glass Struct. Eng.
DOI 10.1007/s40940-016-0018-1

RESEARCH PAPER

The mechanical behaviour of SentryGlas® ionomer and TSSA silicon bulk materials at different temperatures and strain rates under uniaxial tensile stress state

Manuel Santarsiero · Christian Louter · Alain Nussbaumer

Received: 25 January 2016 / Accepted: 29 March 2016

Abstract An innovative type of connections for glass components, called laminated connections, has been developed in the last years. Two materials have been used for laminated connections: the transparent ionomer SentryGlas® (SG) from Kuraray (former Dupont) and the Transparent Structural Silicon Adhesive (TSSA) from Dow Corning. In this paper, the mechanical behaviour of SG and TSSA bulk materials is studied under uniaxial tensile stress condition. The effects of strain rate and temperature variations are investigated. Particular attention is paid (i) to the study of these polymers in cured condition and (ii) to the computation of true stress and strain field during the tests. Firstly, it is observed that the mechanical behaviour of both SG and TSSA are temperature and strain rate dependent. These effects are quantitatively determined in the paper. Secondly, two additional phenomena are observed. For TSSA, it is observed that the material goes from fully transparent to white colour, exhibiting the so-called whitening phenomenon. For SG, instead, it is observed that the strain field distribution is dependent on the temperature. More specifically, the material exhibits a non-uniform strain field distribution due to the occurring of the necking phenomenon. Measurements along the specimens, using Digital Image Correlation techniques, showed that the localized strain propagates over the full specimen length, resulting in a cold-drawing phenomenon. Finally, it is also shown that engineering and true stress–strain definition exhibits large deviation indicating that the finite deformation theory should be used for the computation of the stress–strain curves to be implemented in numerical modelling.

Keywords SentryGlas® ionomer · TSSA silicon · Laminated connections · Polymer · Temperature · Strain rate

M. Santarsiero (✉)
Eckersley O'Callaghan Engineers (EOC), London, UK
e-mail: manuel.santarsiero@gmail.com

M. Santarsiero · A. Nussbaumer
Steel Structures Laboratory (ICOM), School of Architecture, Civil and Environmental Engineering (ENAC), École Polytechnique Fédérale de Lausanne (EPFL), Lausanne, Switzerland
e-mail: alain.nussbaumer@epfl.ch

C. Louter
Chair of Structural Design, Department of Architectural Engineering and Technology (AE+T),
Faculty of Architecture and the Built Environment (A+BE),
Delft University of Technology (TU Delft), Delft,
The Netherlands
e-mail: Christian.Louter@TUDelft.nl

1 Introduction

An innovative type of connections for glass components, called laminated connections, has been developed in the last years (Peters 2007; O'Callaghan and Coult 2007; O'Callaghan 2012; Lenk and Lancaster 2013). This bonding technique makes use of transpar-

Published online: 04 May 2016

ent adhesive materials produced in solid foils to bond metal to glass. The concept of laminated connections is to use the same production process of laminated glass components. Laminated glass components are made of several glass panels bonded together with transparent adhesive polymeric foils. Once together, glass panels and polymeric foils are placed in a vacuum bag and go through an autoclave lamination process. Similarly, in laminated connections, metal, adhesive and glass parts are placed together in a vacuum bag and then go through the same autoclave process as applied for laminated glass components. For the current publication, two materials used for laminated connection are of specific interest: the transparent ionomer SentryGlas® (SG) from Kuraray (former Dupont) and the Transparent Structural Silicon Adhesive (TSSA) from Dow-Corning.

SentryGlas® (SG) is a thermoplastic transparent ionomer used in laminated glass applications as interlayer. The glass transition temperature of SG is approximately 50–55 °C (Decourcelle et al. 2009; Calgeer 2015). Compared to other interlayers for glass applications (e.g. PVB and EVA) SG is characterized by higher stiffness, enhanced durability and higher mechanical resistance. The SG is typically produced in foil thickness of 0.76, 0.89 and 1.52 mm. SG foils are rather rigid at room temperature. In literature, the bulk SentryGlas® material has been investigated under uniaxial stress state by several authors (Bennison 2005; Meissner and Sackmann 2006; Belis 2009; Biolzi et al. 2010; Puller et al. 2011; Schneider 2012; Kuntsche and Schneider 2014). Tests were performed at room temperature and different displacement rates. Nominal or so-called engineering stress–strain definitions are generally used. Limited results are available on uniaxial tensile tests at different temperatures (Puller 2012).

The TSSA material is a Transparent Structural Silicon Adhesive produced by Dow Corning, that has been recently commercialized for laminated connections in structural glass applications. TSSA is an elastomeric one-component addition-cured silicon with no by-products, characterized by nano-silica and cross-linked polymers. Compared to standard silicone adhesives used in glass applications, TSSA exhibits higher stiffness and strength, which makes it suitable for structural applications. It should be noticed that, conversely to SG, TSSA is exclusively intended for metal-to-glass adhesive laminated connections glued to the glass surface. TSSA is not intended neither for embedded laminated connections nor for laminated glass components in general[1]. The glass transition temperature of the polymer is around −120 °C[2]. The curing process is activated by heat and it occurs rather rapidly. Rheometry tests showed that 90 % of the mechanical response is achieved after 15 min at 130 °C (Sitte 2011). TSSA is produced in foils of 1mm thickness. In literature, the available studies on TSSA are mainly focused on connections tested at room temperature (Sitte 2011). Limited studies are performed on TSSA bulk material at different temperature and strain rate. In (Sitte 2011), TSSA bulk material is tested at room temperature and constant displacement rate. Nominal or so-called engineering stress–strain definitions are usually used.

In this paper, the mechanical behaviour of TSSA and SG bulk material is studied under uniaxial tensile stress condition. The effects of strain rate and temperature variations are investigated. The goals of this work are to (i) increase the mechanical understanding of SG and TSSA behaviour in different conditions, (ii) derive the stress–strain curves of SG and TSSA, (iii) investigate the effects of temperature and strain rate and (iv) evaluate the mechanical parameters useful for FEM material modelling (e.g. Young modulus, Poisson's ratio, etc.) as a function of temperature and strain rate. In this work, particular attention is paid to investigate the polymers in cured condition (as such as they are in laminated connections) and to compute stress and strain field distribution using true definitions.

Firstly, the fabrication of specimens and the measurement system are described. A Digital Image Correlation system is used to measure the full strain field distribution during the test. This allows the computation of both longitudinal and transversal deformation up to failure. Secondly, the stress–strain curves and the main mechanical properties such as modulus of elasticity, Poisson's ratio, maximum stress and strain at failure are obtained. The effects of strain rate and temperature variations are then discussed. The differences between true and engineering definition for stress, strain and strain rate are shown for both materials. Finally, two additional phenomena are discussed: the whitening of TSSA and the necking of SG. The first one concerns the change of colour of TSSA once the stress reaches a

[1] This is at the time of writing. The reason might be related to technological and production matters.

[2] P. V. Dow Corning Europe, Personal Communication, July 22th, 2015.

certain value. The second one concerns the local strain intensification that occurs in the SG material at temperatures below 40 °C. Finally, the deviation between local and global strain measurements and the difference between engineering and true stress–strain definition are discussed.

2 Material and method

2.1 Specimens production, measurements system and test setup

Uniaxial tensile tests are performed on dumbbell shaped specimens cut out of laminated SentryGlas® ionomer and TSSA silicon foils. The adhesive foils went through an autoclave process before testing to investigate their material properties in cured condition. Constant thickness and straightness of the specimens must be guaranteed during the lamination. The polymeric foils are therefore placed between two glass plates before lamination. Teflon foils (PTFE) are placed between glass and adhesives foils to avoid the polymers to stick to the glass. The full pack is then vacuumized and laminated in autoclave. The scheme of Fig. 1a describes the specimen preparation. The autoclave protocol is the same used to produce the laminated connections, as earlier discussed in this work. After lamination, dumbbell specimens are cut out of the laminated foils by Computer Numerically Controlled (CNC) cutting machine.

The dumbbell specimens are based on EN ISO 37-type 2 (International Organization for Standardization 2011) which is equal to EN ISO 527-B type 5a (CEN-European Committee for Standardisation 1996). Figure 1b shows the specimens' geometry. In the current study, the transversal dimensions are increased with a factor of 2.5. This permits to have sufficient area for clear observation of necking phenomenon, to have accurate Poisson's ratio measurements and to avoid any sliding in the grips. All the other dimensions are as per EN ISO 37-type 2. The thickness of the SG specimens is 1.5mm. The thickness of TSSA specimens is 1mm.

A Digital Image Correlation (DIC) system is used to compute the full strain field during the tests. Each component of the strain tensor is measured at every location, i.e. vertical elongation, horizontal elongation and shear distortion. These measurements permit to calculate the magnitudes and directions of principal strains, the Poisson's ratio, the actual cross section of the specimens and the actual stress in the specimens during the test. The use of DIC usually requires the application of a random speckle pattern over a white background painted on the specimen surface. However, this is not here applicable due to the large elongation exhibited by the polymers at failure. Indeed, after a certain level of strain, the white paint would detach from the surface and the strain calculation would consequentially fail. To address this issue a different method is here adopted, which makes use of the material transparency. Firstly, only a speckle random pattern is applied on the specimens without background (see Fig. 2). Then a white panel is placed behind the specimens along both cameras axes (see Figs. 3, 4). This method allows to compute the strain field distribution at large deformation level. If not differently specified, strains are always measured in the narrow parallel-sided portion of the specimens as indicated by EN ISO 38 and EN ISO 527, depicted by Fig. 1 by l_1 and here defined as initial *specimen length*.

All specimens are conditioned for at least 24h before being tested in a conditioned room at 23 ± 1 °C and 50 ± 10 % R.H., according to the indication of the guideline ETAG 002 (European Organisation for Technical

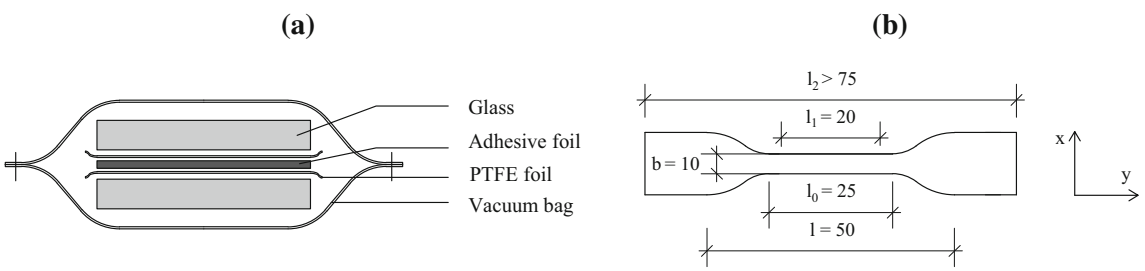

Fig. 1 **a** Scheme of the preparation and lamination of specimens in cross section **b** dimension of the specimens (dimensions in mm)

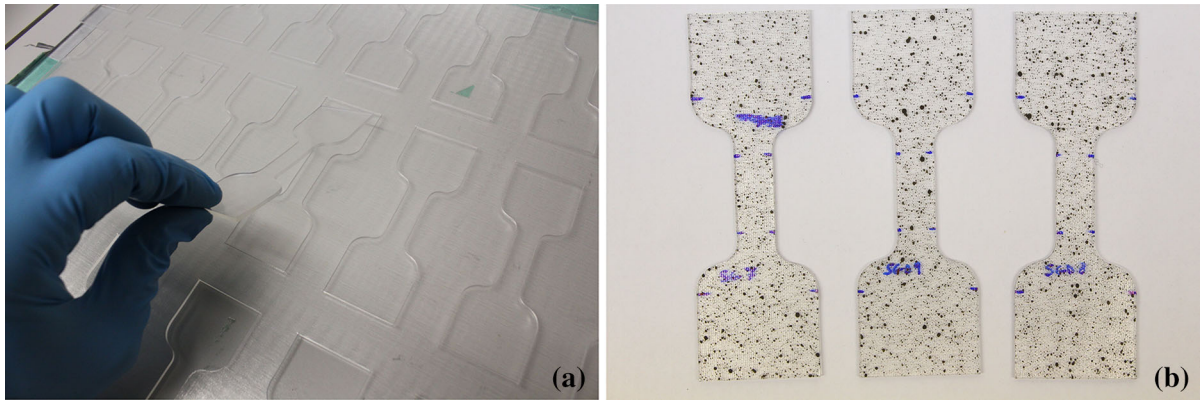

Fig. 2 **a** Dumbbell specimens after lamination and CNC cutting **b** Dumbbell specimens with random speckle pattern painted on the surface

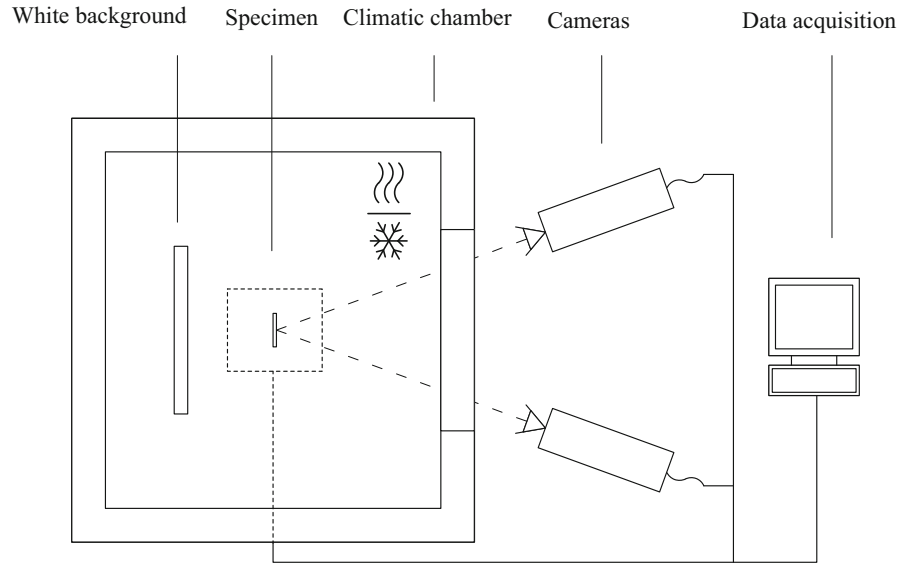

Fig. 3 Scheme of test setup and measurement system—plan view

Approvals 2001). Tests are performed with a 50 kN Universal Testing Machine (see Fig. 5). The testing machine is equipped with two additional small load cells, given the small loads values to be measured during the tests. Load cells of 1 and 0.5 kN were used for the SG and the TSSA respectively. The testing machine is equipped with a climatic chamber for a temperature range of −30 and +80 °C, with a temperature resolution of ±0.1°C. Constant airflow during all tests is ensured in the climatic chamber by internal fans. The standard ASTM 412-06a on uniaxial tensile test (American Society for Testing and Materials 2008) indicates to maintain specimens in the climatic chamber at constant temperature for at least 10 min before testing. Because of the high temperature sensitivity of the materials under investigation, specimens are here kept at constant temperature for at least 30 min before testing to ensure uniform temperature in the specimens.

2.2 Test configurations

According to the guideline ETAG 002 (European Organisation for Technical Approvals 2001), −20[3] and 80 °C can be considered as temperature limits for practical purpose in civil engineering, while 23 °C is considered as reference value. According to this indica-

[3] According to ETAG 002 low temperature limit could be extended to −40 °C for European Nordic countries if required. This is not here considered because of practical limitation.

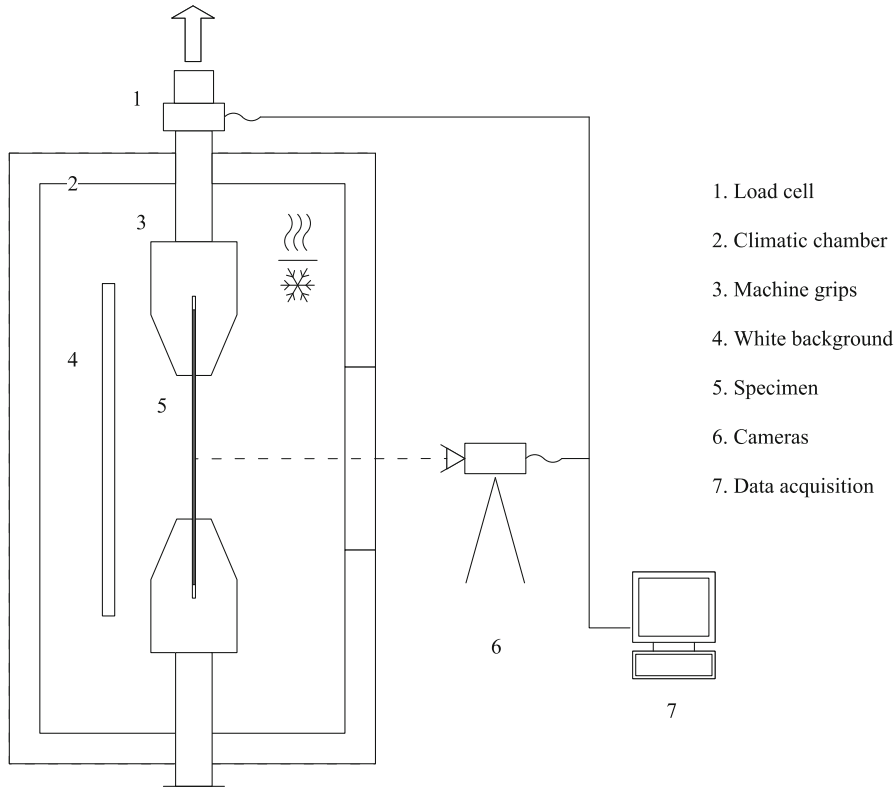

Fig. 4 Scheme of test setup and measurement system—lateral view

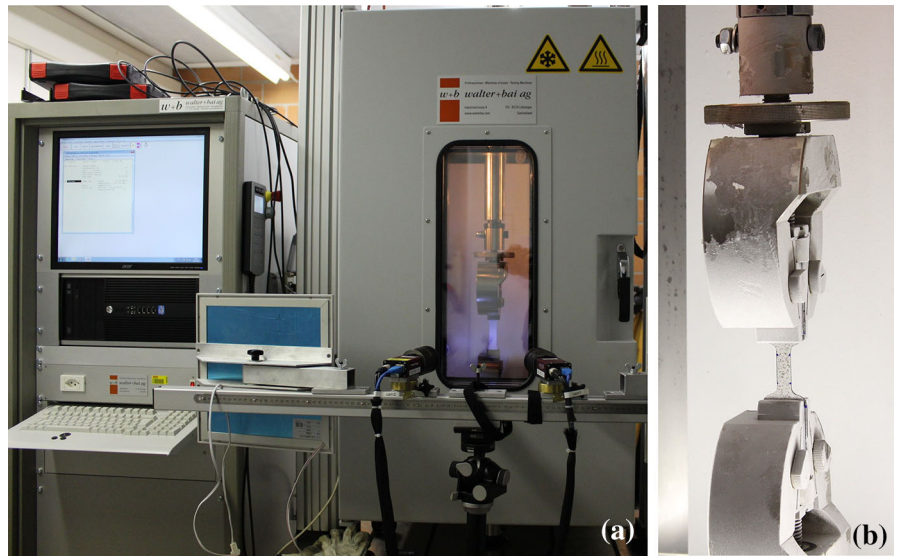

Fig. 5 **a** Tensile testing machine with climatic chamber and DIC measurement system **b** Dumbbell specimen in the grip inside the climatic chamber

tion, TSSA silicon is tested at −20, 23 and 80 °C. SG instead is tested at seven different temperatures within this range: −20, 0, 23, 30, 40, 60 and 80 °C. SG is tested at more temperatures due to its expected high temperature sensitivity. This is because its glass transition temperature, T_g, falls within this temperature range (i.e. $T_g \cong 50$–55 °C) (Decourcelle et al. 2009; Calgeer 2015).

Both materials are then tested at three different crosshead machine displacement rates, in this work indicated as $\dot{d}$: 1, 10 and 100 mm/min. Tests at 10mm/min are repeated three times at the same config-

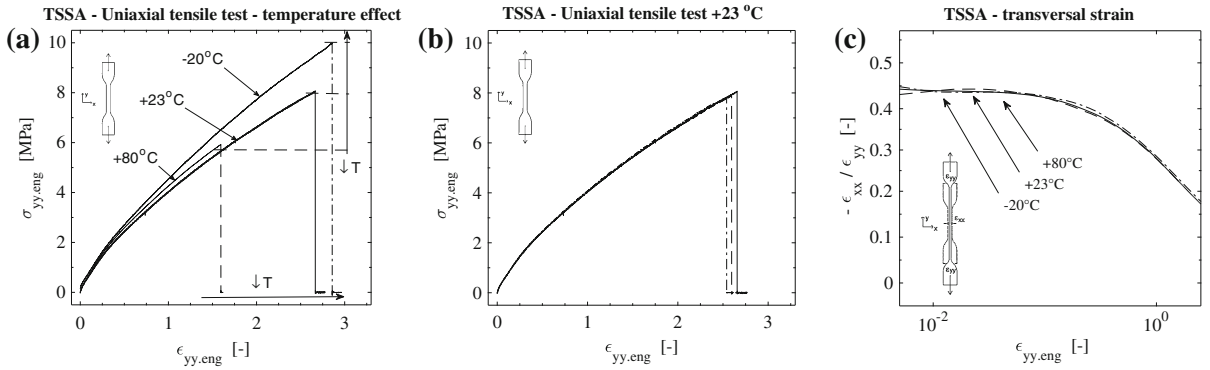

Fig. 6 **a** TSSA behaviour at −20, 23 and 80 °C at 10 mm/min. The *bottom* and *right sides arrows* indicate variation of maximum values as a function of temperature variation **b** TSSA uniaxial tensile stress–strain curves at 23 °C—three tests **c** TSSA transversal-longitudinal strain ratio versus longitudinal strain at different temperatures

uration to evaluate results variability. These displacements rates are defined based on practical limitation of the machine. Further tests at very high displacement rate (e.g. m/s) should be performed to evaluate the mechanical response of TSSA and SG in case of impact or blast scenario.

3 Results

This section collects the test results of TSSA and SG behaviour under uniaxial tensile stress. The $x - y$ reference system is defined with y along the vertical axis (parallel to the testing direction) and x along the horizontal axis (orthogonal to the testing direction) (see Fig. 1). Herein, longitudinal stress and longitudinal strain are here called as σ_{yy} and ε_{yy}, while transversal strain is defined as ε_{xx}. The convention of positive strain for material elongation and negative for contraction is here assumed. In the parallel narrow section of the specimen the directions of y and x axes coincide with the principal directions.

In the following sections the results are expressed, unless otherwise specified, in terms of nominal stress and strain, also known as engineering stress and engineering strain. Engineering stress is defined as the ratio between actual force, F, and initial cross section of the specimens, A_0 (see Eq. (1)). Engineering strain is defined as the ratio between length variation, Δl, and initial specimen length under consideration, l_1 (see Eq. (2)). The longitudinal stress–strain curves are presented for different temperatures and displacement rates. The correlation between displacement rate and strain rate is later calculated in the following section on results analysis. The ratios between transversal strains and longitudinal strains are also plotted with respect to the longitudinal strain.

$$\sigma_{eng} = \frac{F}{A_0} \tag{1}$$

$$\varepsilon_{eng} = \frac{\Delta l}{l_1} \tag{2}$$

3.1 TSSA uniaxial tensile behaviour at different temperatures and displacement rates

This section presents the results of the uniaxial tensile tests on TSSA silicon. The stress–strain curves of TSSA and the effects of temperature and displacement rate variations are presented.

Figure 6a shows the response of TSSA at −20, 23 and 80 °C. The stress–strain curve firstly exhibits a short linear behaviour up to engineering stress approximately equal to 2 MPa. This is then followed by nonlinear behaviour that continues up to failure. The material seems to exhibit hyperelastic behaviour, confirming preliminary results of (Sitte 2011). Tests repeated in the same configuration (see Fig. 6b) give similar results with limited variation. Initial stiffness and the stress–strain curve are not significantly affected by temperature. This is in line with expectation since the glass transition temperature of silicon is below the investigated range of temperature. It is observed that the 80 °C curve is comprised between 23 and −20 °C curves. Further tests should be performed to assess if this is due to statistical variation or a temperature effect. The maximum stress and strain are observed to be temperature dependent. If compared to the one at 23 °C, the maximum

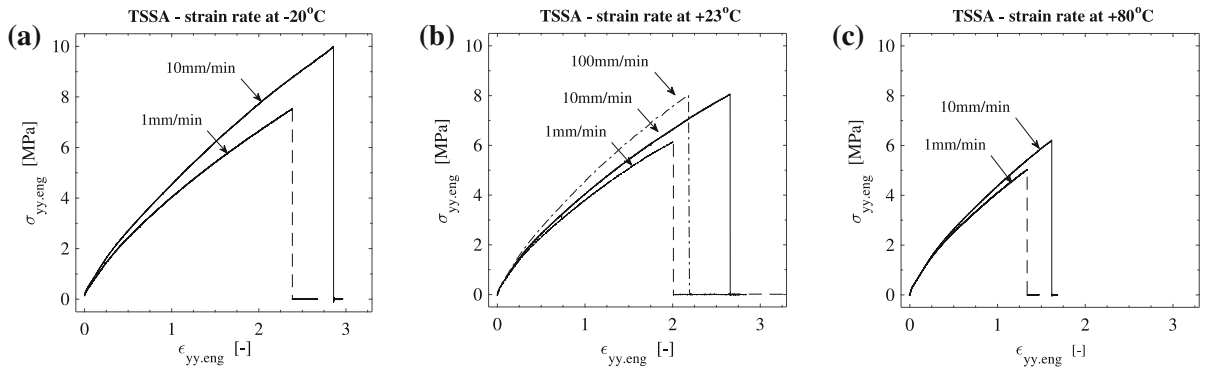

Fig. 7 Effects of displacement rate on TSSA silicon at different temperature: **a** −20 °C **b** 23 °C **c** 80 °C

stress at failure increases when the temperature goes down to −20 °C and decreases when temperature goes up to 80 °C. The maximum strain also increases at low temperature and decreases at high temperatures.

Figure 6c shows the behaviour of transversal strain over time for TSSA material at different temperatures. The results are expressed in terms of ratio between transversal and longitudinal strain. This ratio corresponds to the definition of Poisson's ratio. The curves firstly show a constant horizontal behaviour around a value of 0.44. At large deformation, the ratio decreases linearly with the logarithm of the longitudinal strain. The effects of temperature variation appear to be negligible.

The graphs of Fig. 7 show the effects of the displacement rate on the TSSA behaviour. Stress–strain curves at 10mm/min and 1mm/min are presented for −20, 23 and 80 °C. For TSSA at 23 °C, 100mm/min displacement rate is also investigated. Comparing curves at 1mm/min to the one at 10mm/min one observes that at 23 °C the maximum stress and strain at failure increase when the displacement rate increases. Similar behaviour is observed at high and low temperature (+80 and −20 °C). The maximum stress at 100mm/min does not differ significantly from what is observed at 10mm/min. However, further tests appear to be necessary to confirm this observation in a rigorous manner.

3.2 SG uniaxial tensile behaviour at different temperature and displacement rates

This section presents the results of the uniaxial tensile tests on SG ionomer. The stress–strain curves of SG and the effects of temperature and displacement rate variations are presented.

Figure 8a shows the response of SG at −20, 0, 23, 30, 40, 60 and 80 °C. All curves initially exhibit a linear behaviour at any temperature. The slope of the curve decreases as temperature increases (see Fig. 8b). Then, each curve shows large non-linear behaviour up to failure. However, the shape of the curve depends on the temperature. Two behaviour types can be distinguished: (i) SG response at temperature above or equal to 40 °C and (ii) SG response at temperature below 40 °C. For a temperature above or equal to 40 °C the curve gradually tends to a plateau value where large deformation occurs. This is then followed by a strain hardening behaviour up to failure. For temperature below 40 °C instead, it is possible to observe a clear yielding stress, defined as the relative maximum occurring after the linear part. After this relative maximum, the stress–strain curve exhibits a softening branch. This is then followed by a hardening behaviour. The maximum stress at failure is usually comparable or larger than the yielding stress. This behaviour of SG at temperatures below 40 °C is in line with results in literature (Puller et al. 2011) and it is common for polymeric material in the so-called "glassy state" i.e., adhesives at temperature below their glass transition temperature.

Figure 8c shows the behaviour of transversal strain over time for SG material at different temperatures. The results are expressed in terms of ratio between transversal and longitudinal strain. This ratio corresponds to the definition of Poisson's ratio. The curves firstly show a constant horizontal behaviour. Here, the Poisson's ratio value falls in the range of 0.4–0.5 and it is temperature dependent. It is about 0.4 for low temperature and tends to 0.5 when temperature increases. In case of large deformation, the ratio decreases linearly with the logarithm of the longitudinal strain.

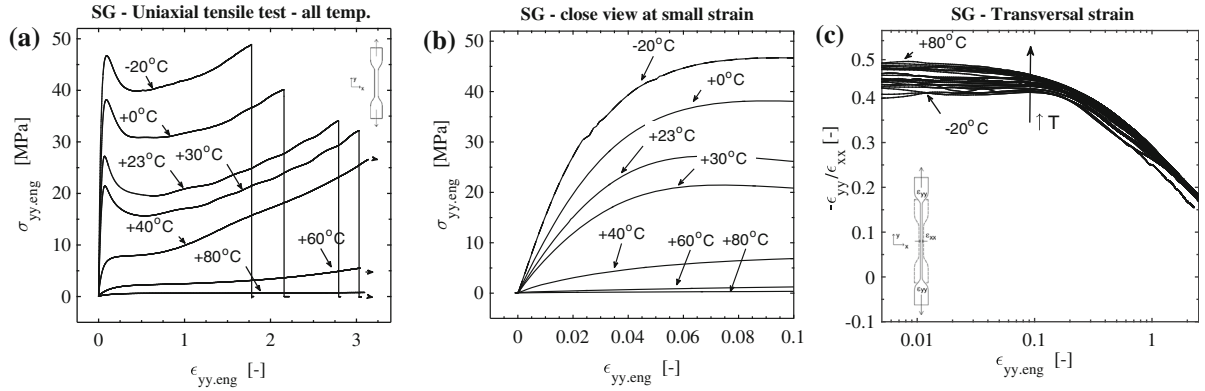

Fig. 8 **a** SG uniaxial tensile behaviour between −20 and +80 °C at 10 mm/min **b** Close view on the initial part of the stress–strain curves at different temperatures **c** SG transversal-longitudinal strain ratio versus longitudinal strain at different temperatures. *Lower line* is the result at −20 °C and *upper line* is the result at +80 °C. *Intermediate lines* are the results at intermediate temperatures

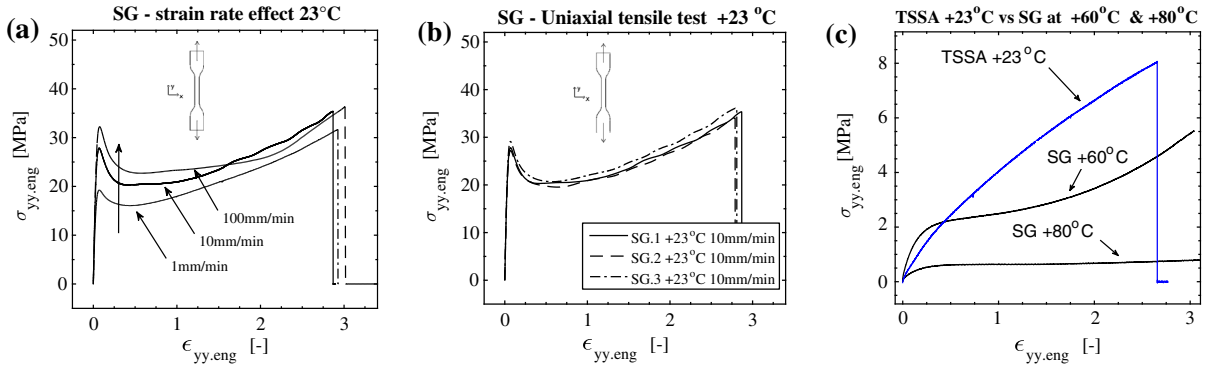

Fig. 9 **a** Strain rate effect on the behaviour of SG under uniaxial tensile test at 23 °C **b** SG uniaxial tensile stress–strain curves at 23 °C and 10 mm/min—three tests **c** Comparison between TSSA and SG stress–strain curves

The yielding stress and the maximum stress at failure are strongly temperature dependent. The yielding stress and the maximum stress at failure increase when temperature decreases. The maximum strain at failure instead decreases when temperature decreases, going from more than 300 % to 70 %. For temperatures above 40 °C the maximum displacement capacity of the machine is reached before failure. Tests repeated in the same configuration (see Fig. 9b) give similar results with limited variation. However, comparison between SG and TSSA (Figs. 6b, 9b) denotes that the silicon variation is smaller than the ionomer one. For the sake of comparison, Fig. 9c shows TSSA and SG curves at high temperature.

Figure 9a shows the effects of displacement rate on SG at 23 °C. It is observed that the displacement rate has an important effect on the yielding stress. Indeed, higher and smaller displacement rates cause respectively larger and smaller yielding stress. The effect of the displacement rates on the maximum stress at failure is instead more limited.

4 Analysis of results

4.1 Necking effect on SG

A relevant difference between the SG ionomer behaviour at high and low temperatures is observed by analysing in detail the strain field distribution during the test. Figure 10 shows the strain field distribution computed by DIC during the tests. For temperatures equal to or above 40 °C the strain field distribution is uniform along the specimens length for both small and large strain range (Fig. 10a) (where *specimens length*

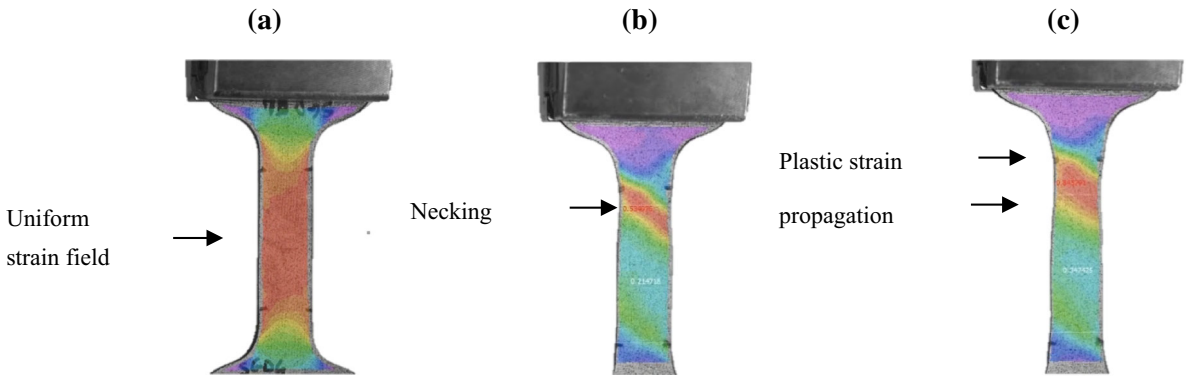

Fig. 10 Photos of SG specimens during tests at low and high temperature, overlapped with strain field obtained by DIC. **a** Test at 80 °C: uniform strain distribution (**b**). Test at 23 °C: Local plastic strain concentration at yielding point and consequent necking effect **c** Test at 23 °C: necking effect and start of the plastic strain propagation along the specimen length

is the narrow parallel-sided portion of specimens indicated Fig. 1 by l_1). On the contrary, for temperatures below 40 °C, the strain field behaviour is more complex. Indeed, for small strain values (i.e. elastic region) the strain field distribution is uniform (such as shown in Fig. 10a). When stress increases and approaches the yielding point, a local strain concentration starts to occur (Fig. 10b).

Then, when the strain increases, the concentration becomes more important and visible. This results in a local region of high concentration of longitudinal stress and strain (Fig. 10c). Due to the Poisson's effect, also the transversal strains are larger in this local region than in the rest of the specimens. Consequently, the actual width in this region is much smaller than in the rest of the specimens. This effect, also as known *necking effect* (Ehrenstein 2001), is clearly visible even with the naked eye, and occurs for all tests performed below 40 °C. The necking effect corresponds to the softening phase of the stress–strain curve.

After the yielding point, the locally plastified region starts to propagate over the whole length of the specimen (see Fig. 13), phenomenon also known as *cold drawing* (Ehrenstein 2001; Roylance 1996). When the plastic propagation is fully extended, which corresponds to the beginning of the hardening phase, the strain field is uniform again and increases until failure.

The necking effect is observable also from Fig. 11. The latter shows the longitudinal strain versus time in case global measurement (average along the specimens length) or local measurement (locally measured in the necking region). Firstly, there is an initial linear behaviour, i.e. constant strain rate over time, where global and

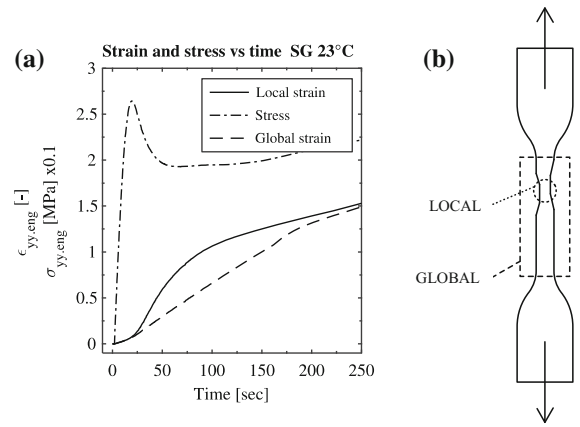

Fig. 11 **a** Local strain, global strain and stress versus time for SG at 23 °C **b** Scheme of the local and global measurements

local measurements give same results. Once the yielding stress is reached the two strain curves deviate. The local strain increases more rapidly if compared to the global one. This phenomenon corresponds to the strain intensification that occurs in the necking region mentioned above. Once the necking has propagated along the full specimens length, the two curves tend again to have similar behaviour. This corresponds with the start of the hardening phase of the stress–strain curve. The propagation of the necking effect is also shown by Fig. 12. More specifically, Fig. 12a shows the measurements of the longitudinal strain at different location along the specimen versus time.

From the aforementioned consideration it follows that for material exhibiting necking behaviour local strain measurement in the necking region should be

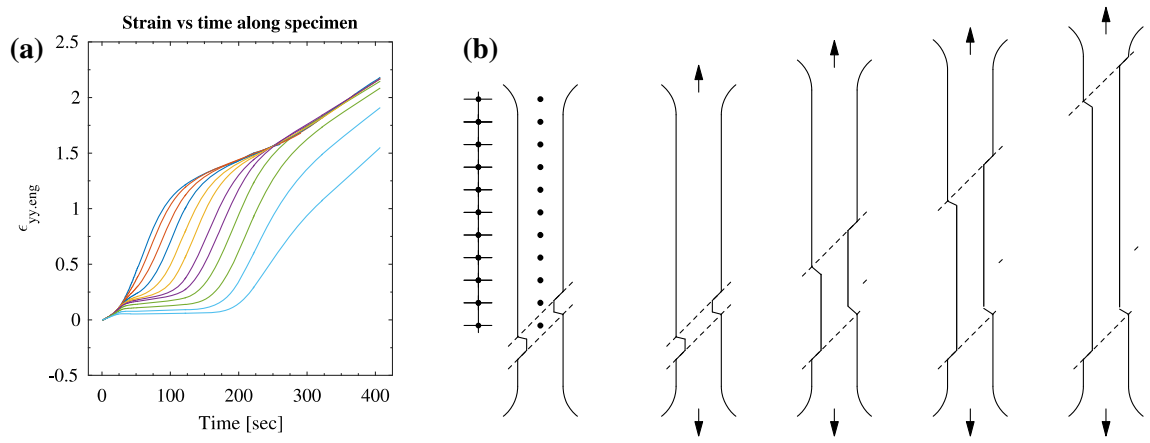

Fig. 12 **a** Local strain measured during the tests over time at different location along the SG specimens at 23 °C with increasing ordinate position, i.e. starting from the necking region to the end of the specimen **b** Scheme of the necking propagation and measurement locations

preferred, as it is done in the present work. This allows obtaining the real local material behaviour rather then global response of the specimens[4]. When the necking is not occurring, global and local strain measurements give identical results. In this case, material properties can be directly implemented from the global measurement.

The hardening effect, i.e. increase of stress with plastic strain propagation, could be related to a more ordered state of the polymer chains network once subjected to large stretching (Ehrenstein 2001; François et al. 2013). Indeed, once untangled, polymer chains tend to offer more resistance against further stretching, and therefore hardening behaviour (Fig. 13).

Furthermore, the necking effect is consistently occurring with a particular shape. The strain intensification is approximately oriented at a 45° inclination with respect to the longitudinal testing direction. This indicates that the deviatoric component of the stress tensor plays an important role in the plastification of the SG below 40 °C. Indeed, the shear stress in a continuum homogeneous isotropic material under uniaxial tensile stress state is maximum along a plane at 45° with respect to the tensile stress direction. This consideration appears to be in line with the observation. Similar behaviour is observed for metal under uniaxial

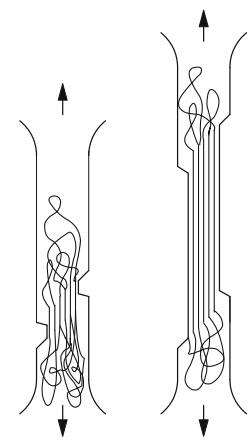

Fig. 13 Necking effect and polymer chains ordering

tensile stress at yielding. In that case, the 45° bands of strain concentration are also called *Lüders band* (Pelleg 2008). One of the main causes behind the yielding phenomena in metallic materials is the movement of dislocations. In the case of SG, the yielding could be related to the movement of polymer chains dislocations (Roylance 1996; Pelleg 2008), with subsequent cold drawing and hardening response, rather then dislocation movement of metallic crystal.

In ionomer materials, like SG, additional ionic groups are attached to the polymer chains (Eisenberg and Rinaudo 1990; Macknight and Earnest 1981; Varley 2007). These ionic groups are then attracted to each other due to their chemical reactivity resulting in additional bonds between the polymeric chains (Fig. 14). These bonds increase the material stiffness and strength

[4] In case of local measurement are not possible, inverse material characterization is suggested. This should be done either with user-choice based method or using automatic iterative algorithms with statistical convergence criteria.

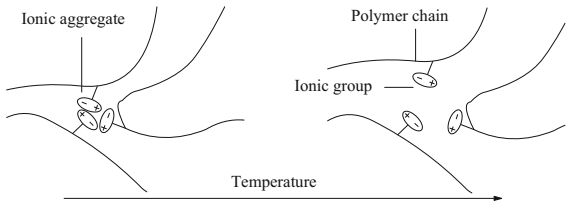

Fig. 14 Scheme of ionic group mechanism on ionomer chains at different temperatures

since additional resistance against stretching of the polymeric network is provided. It follows that, when the material is subjected to tensile stress, the presence of these ionic groups make the stretching of polymer network less favourable than the sliding of polymer chains over each other. This could explain the role of the deviatoric stress on SG yielding and the 45° inclination of necking phenomenon, at temperature below 40 °C. If external energy is provided to the material (e.g. heat source) the bonds can be overcome more easily with a subsequent decrease in stiffness and yielding stress. Consequently, the polymeric chains show less resistance against network stretching at high temperature, which could explain the uniform strain distribution at temperature >40 °C.

4.2 Whitening effect of TSSA

The SG ionomer and TSSA silicon are fully transparent polymers after curing. However, it is observed that the TSSA silicon does not remain transparent for the whole test duration. Indeed, when TSSA overcomes a certain stress level, its colour changes from fully transparent to white. In order to observe this phenomenon a not painted specimen (i.e. without speckle pattern) is tested using black paper as background. Figure 15 shows the whitening phenomenon evolution with increasing stress level. The whitening phenomenon starts to be visible in a clear manner at engineering stress around 5 MPa. This confirms the preliminary results observed in (Sitte 2011). However, it should be noticed that the whitening phenomenon in TSSA under uniaxial tensile stress occurs in a gradual manner. It is therefore hard to clearly distinguish the beginning of the whitening with the naked eyes. Once the test starts, very small white points appear even at low stress level (e.g. Fig. 15b). Then, when the stress increases, the density of the points increases and the transition from transparent to white is clearly visible[5] (e.g. Fig. 15c).

4.3 Finite deformation theory and true stress–strain

The definitions given by Eqs. (1) and (2) in the previous section belong to the infinitesimal strain theory of continuum mechanics. It assumes the hypothesis of modulus of displacements and its first gradient to be largely smaller than the unit in each point of the body. The deformed and non-deformed configurations of the body can be therefore considered coincident.

Due to the large elongation that SG and TSSA exhibit, the hypotheses of the infinitesimal strain theory are no longer valid for the entire test duration. For instance, the difference between the actual cross section and the initial one is not negligible anymore. In this case, the finite deformation theory applies. It follows that the actual stress (called *true stress*) and the actual strain (called *true strain*) are defined by (3) and (4) instead of (1) and (2). In (3) and (4), l is the actual length and A is the actual cross section area.

$$\sigma_{true} = \frac{F}{A} \tag{3}$$

$$\varepsilon_{true} = \int \frac{\partial l}{l_0} = ln\left(\frac{l}{l_0}\right) = ln\left(1 + \frac{\Delta l}{l_0}\right) = ln\left(1 + \varepsilon_{eng}\right) \tag{4}$$

$$A = A_0\left(1 + \varepsilon_{xx}\right)^2 \tag{5}$$

The actual cross section area, A, is computed by means of Eq. (5), i.e. accounting the transversal strain occurring due to the Poisson's effect and the related material contraction. As stated before, it is assumed the convention of positive strain to indicate elongation while negative strain indicates contraction. In case of very small deformations, both finite and infinitesimal theory definitions give similar results and A tends to A_0.

In the previous sections it is shown that SG and TSSA under uniaxial tensile stress state develops large deformations before failure. It follows that the finite strain theory should be applied for SG and TSSA instead of the infinitesimal one. This means that *true stress* and *true train* should be used. For the sake of

[5] In case of different test typologies that induce different stress states, the whitening load can occur in a more distinguishable manner, see (Santarsiero 2015; Sitte 2011; Hagl et al. 2012).

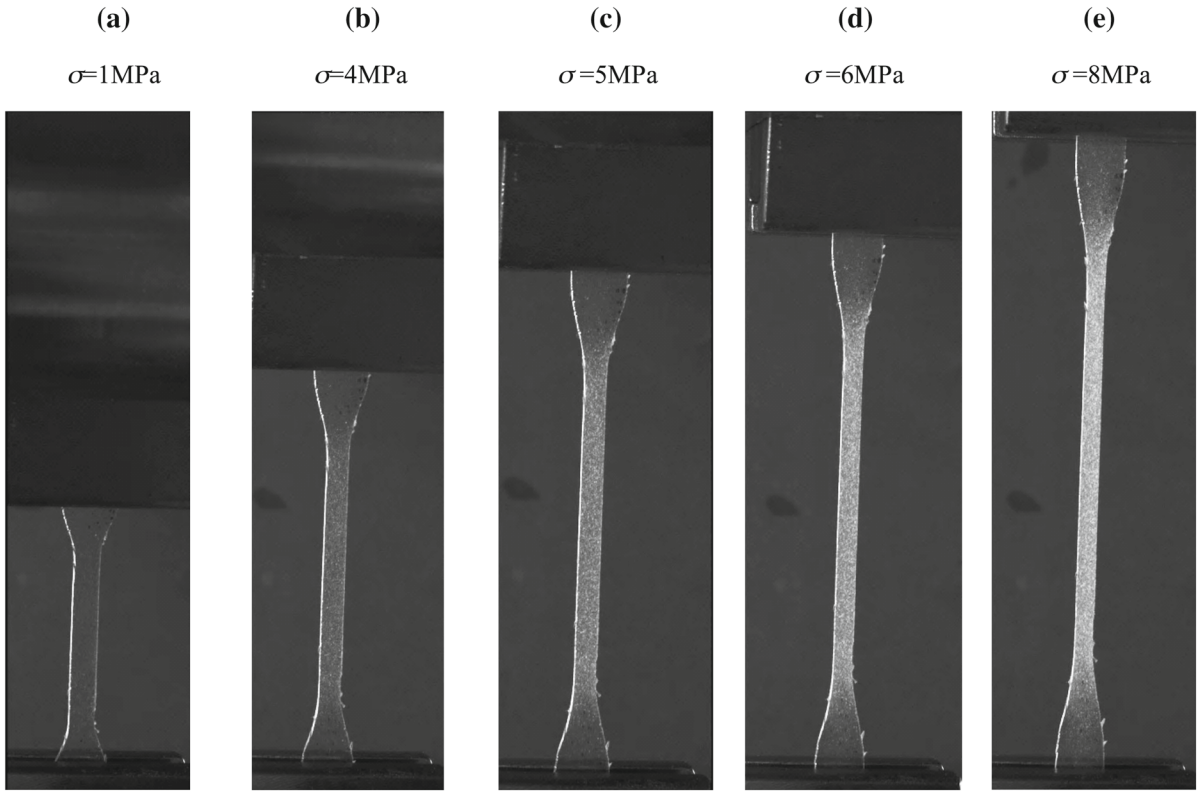

Fig. 15 Whitening effect of TSSA at different stress level under uniaxial tensile stress

example, in Fig. 16 SG stress–strain curves are plotted using either engineering or true definitions. It can be seen that, for large deformation, both stress and strain values show large differences between engineering and true values. As expected, this difference reduces in case of small deformation and it tends to zero for very small deformation (see close view at elastic part of Fig. 16b).

Figure 17 shows then the ratio between transversal and longitudinal strain measured during the test of SG and TSSA. Two types of curves are computed: one according to the engineering strain definition of Eq. (2) and one according to the true strain definition of Eq. (4). At the beginning (i.e. low deformation), the two curves show similar constant horizontal behaviour. Once the strain increases, the two curves start to deviate. The curves with true definition do not decrease as the engineering one but gradually tend to a value of 0.5. This confirms that true strain definition should be used. Indeed, in case of plastic deformation, it is commonly assumed to have no volume changes in the material during the plastic strain flow. This means, in the case of uniaxial tensile test, ratio between transversal and longitudinal strain close to 0.5, which is in line with the experimental observation.

4.4 Mechanical material properties

The maximum stress at failure, the maximum strain at failure, the modulus of elasticity and Poisson's ratio are here calculated and plotted as a function of temperature. The applied strain rates correspondent to the applied displacement rates are calculated for each test. This is done computing the first derivative of the strain, measured by means of the digital image correlation system, with respect to the time variable. It is computed that the ratio between applied strain rate and applied displacement rate is equal to 0.024 [−/mm].

Table 1 summarizes the values of the mechanical material properties of TSSA. The maximum stress at failure, $\sigma_{yy,max}$, the maximum longitudinal strain at failure, $\varepsilon_{yy,max}$, the modulus of elasticity, E, and the Poison's ratio, v, are calculated. Maximum stress and maximum strain at failure are computed using both

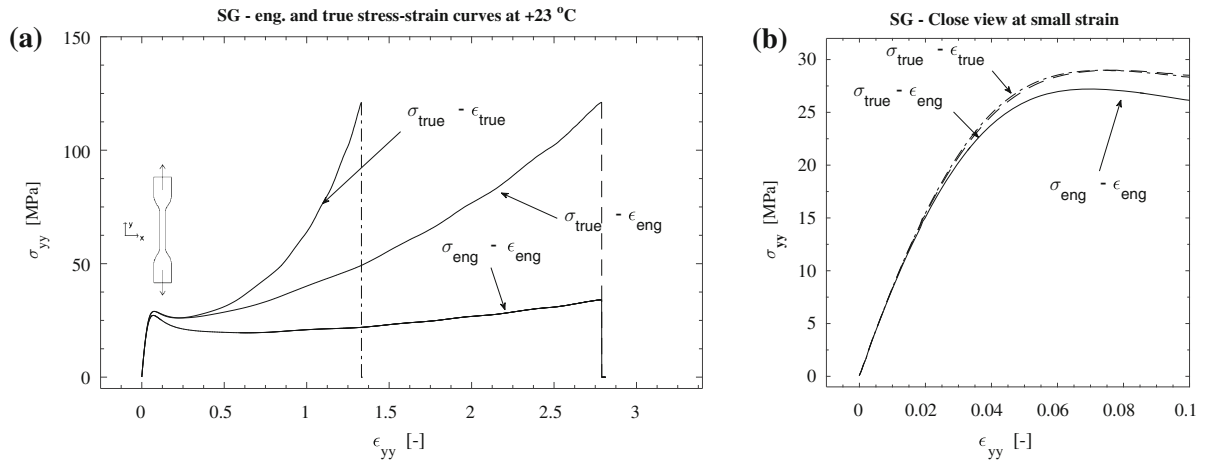

Fig. 16 **a** Engineering and true stress–strain curve of SG at 23 °C **b** Zoom on the elastic part at low strain level

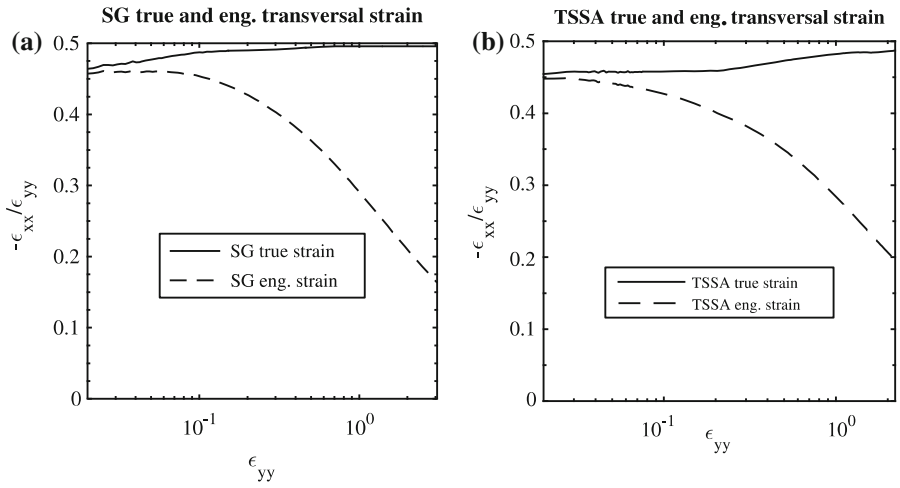

Fig. 17 Behaviour of true and engineering transversal-longitudinal strain ratio for SG and TSSA

engineering and true definitions. The full set of results is given in Appendix Table 4, 5, 6.

In Fig. 18a the behaviour of the TSSA maximum stress at failure is plotted against temperature, going from −20 to +80 °C. Circular and triangular points represent failure at 1 and 10 mm/min respectively. The maximum stress at different temperature varies in the range of 6–10MPa. If compared to 23 °C, the maximum stress decreases about 23 % at 80 °C and increases about 22 % at −20 °C. Stress–temperature trend appears to follow a linear relationship. Similar behaviour is measured for both displacement rates. The behaviour at lower displacement rate is similar to the behaviour at high displacement rate, but shifted downwards with a reduction factor around 20 %. Fig. 18b shows instead the maximum TSSA strain at failure for the same range of temperature. Here it is also observed that the maximum strain increases at low temperature[6]. Fig. 19a and b show the effect of temperature on the modulus of elasticity, E, and Poisson's ratio, v, respectively. It is observed that temperature variations have limited effects on E and v at any strain rate. This is because the TSSA T_g is out of the investigated range of temperature. The modulus of elasticity is around 6.6MPa and the Poisson's ratio around 0.44.

Table 2 summarises the values of the mechanical material properties for SG. The maximum stress at failure, $\sigma_{yy,max}$, the maximum longitudinal strain at failure, $\varepsilon_{yy,max}$, the modulus of elasticity, E, and the

[6] A second order polynomial seems to provide a better fit than linear one.

Table 1 Mechanical material properties of TSSA at different temperatures and engineering strain rates

T (°C)	$\dot{d}$ (mm/min)	$\dot{\varepsilon}$ (−/s)	E (MPa)	v (–)	$\sigma_{yy.max}$ (MPa)	$\sigma_{yy.max.true}$ (MPa)	$\varepsilon_{yy.max}$ (–)	$\varepsilon_{yy.max.true}$ (–)
80	1	4E−04	6.79	0.46	5.00	10.91	1.33	0.85
23	1	4E−04	6.23	0.44	6.13	15.89	1.99	1.09
−20	1	4E−04	6.39	0.46	7.52	23.39	2.21	1.17
80	10	4E−03	6.95	0.45	6.06	14.68	1.60	0.95
23	10	4E−03	6.45	0.44	7.87	21.31	2.58	1.28
−20	10	4E−03	6.57	0.44	9.57	31.70	2.82	1.34
23	100	4E−02	7.10	0.46	8.02	22.80	2.13	1.11

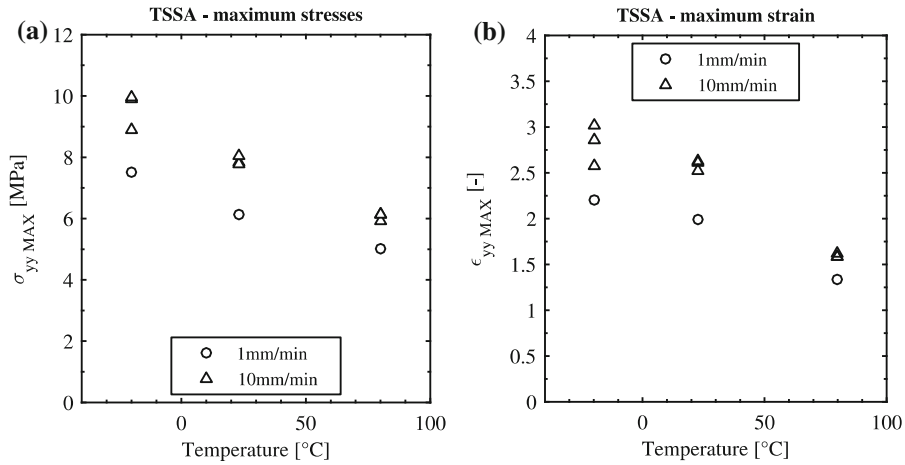

Fig. 18 **a** Effect of temperature variation on TSSA maximum stress **b** Effect of temperature variation on TSSA maximum strain

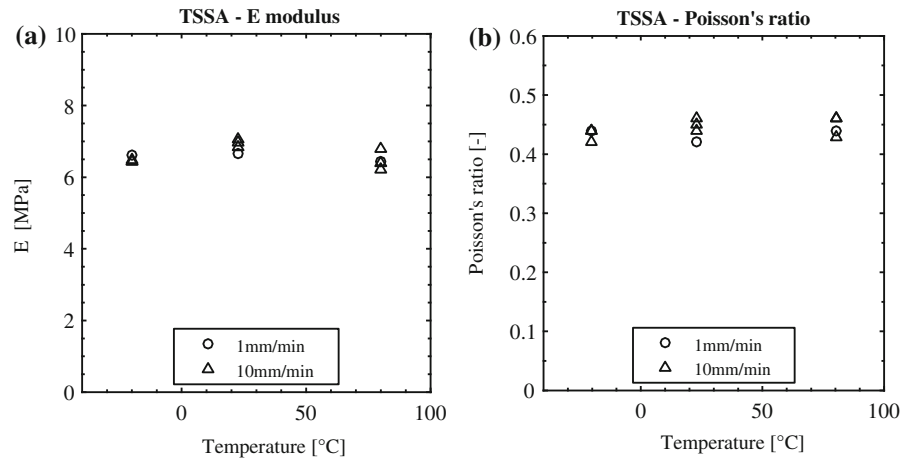

Fig. 19 **a** Effect of temperature variation on TSSA elastic modulus **b** Effect of temperature variation on TSSA Poisson's ratio

Poison's ratio, v, are calculated. Maximum stress and maximum strain at failure are computed using both engineering and true definitions.

Additionally, the yielding stress, here indicated with σ_y, is calculated and collected in Table 3. Two definitions for the yielding stress are used. When possible, the yielding stress is computed as the maximum stress occurring in the stress–strain curve before the softening phase. However, starting from a temperature of 40 °C, the softening phase is not occurring and therefore the yielding stress is not clearly identifiable. In these cases a second definition is used. The yielding stress, σ_{y02}, is calculated following the offset method indicated in (Silva 2012; CEN-European Committee for

Table 2 Mechanical material properties of SG at different temperatures and engineering strain rates

T (°C)	$\dot{d}$ (mm/min)	$\dot{\varepsilon}$ (−/s)	E (MPa)	v (–)	$\sigma_{yy.max}$ (MPa)	$\sigma_{yy.max.true}$ (MPa)	$\varepsilon_{yy.max}$ (–)	$\varepsilon_{yy.max.true}$ (–)
40	1	4.E−04	37.65	0.47	14.21	42.82	n/a	n/a
23	1	4.E−04	505.52	0.43	29.88	120.16	2.86	1.35
−20	1	4.E−04	966.19	0.41	39.49	99.39	1.62	0.96
80	10	4.E−03	3.13	0.49	0.73	3.08	n/a	n/a
60	10	4.E−03	13.53	0.49	5.00	18.68	n/a	n/a
40	10	4.E−03	86.26	0.48	22.80	83.64	3.61	1.53
30	10	4.E−03	498.96	0.44	31.24	118.01	2.98	1.38
23	10	4.E−03	670.21	0.43	32.97	117.34	2.77	1.33
0	10	4.E−03	864.11	0.41	38.33	113.81	2.12	1.14
−20	10	4.E−03	1012.58	0.40	44.96	167.45	1.70	0.99
23	100	4.E−02	700.96	0.43	34.47	136.54	3.00	1.39

n/a Stroke machine capacity is reached for temperature above 40 °C. Only one specimen at 40 °C failed before stroke capacity

Table 3 Mechanical material properties of SG: yielding stress at different temperatures and engineering strain rates

T (°C)	$\dot{d}$ (mm/min)	$\dot{\varepsilon}$ (−/s)	σ_y (MPa)	σ_{y02} (MPa)
40	1	4.E−04	n/a	2.77
23	1	4.E−04	19.62	19.00
−20	1	4.E−04	42.77	35.82
80	10	4.E−03	n/a	0.64
60	10	4.E−03	n/a	2.18
40	10	4.E−03	n/a	5.28
30	10	4.E−03	22.28	20.79
23	10	4.E−03	28.66	27.45
0	10	4.E−03	39.33	35.71
−20	10	4.E−03	48.35	40.72
23	100	4.E−02	32.92	28.43

Standardisation CEN-European Committee for Standardisation; Raghava and Caddell 1973; Raghava et al. 1973; Gottstein 2004). The stress value is calculated as the interception between the stress–strain curve and a straight line starting at strain equal to 0.2 % and with slope equal to the modulus of elasticity.

In Fig. 20a the behaviour of the SG maximum stress at failure is plotted against temperature, going from −20 to +80 °C. Circular and triangular points represent failure at 1mm/min and 10mm/min respectively. The maximum stress at failure decreases at high temperature. A significant drop in the graph is observed when the temperature goes above 40 °C. Results at 1 mm/mm and 10 mm/min shows similar trend but are shifted downwards for low displacement rate. The value of maximum stress at failure goes from 50 MPa at −20 °C to around 0.8 MPa at 80 °C. The maximum strain at failure instead increases with the temperature, as it is shown by Fig. 20b. The relationship between maximum strain and temperature appears to follows a linear law. For temperature above 40 °C the machine stroke capacity is reached and therefore the related values are not plotted. The effects of strain rate on the maximum strain at failure appear to be limited.

The modulus of elasticity of the SG is dependent on the temperature, as shown by Fig. 21a. It goes from a value of around 1000 MPa at −20 °C to around 3 MPa at 80 °C. These results confirm and extend the values given by (Bennison 2005; Stelzer 2010). The modulus of elasticity versus temperature exhibits a behaviour similar to the maximum stress at failure: going from −20 to 80 °C a first gradual decrease with temperature can be observed, followed by a significant drop when temperature overcomes 40 °C. This is in line with expectation because above 40 °C the material is approaching the glass transition temperature that correspond to the material softening.

Figure 21b shows the effect of temperature on the Poisson's ratio. The latter varies in the range of 0.4–0.5. In particular, the Poisson's ratio goes from around 0.4 at −20 °C and approaches 0.5 at high temperature. This is explained by the fact that above 40 °C the material goes from glassy state to rubber state, typically characterized by incompressible behaviour.

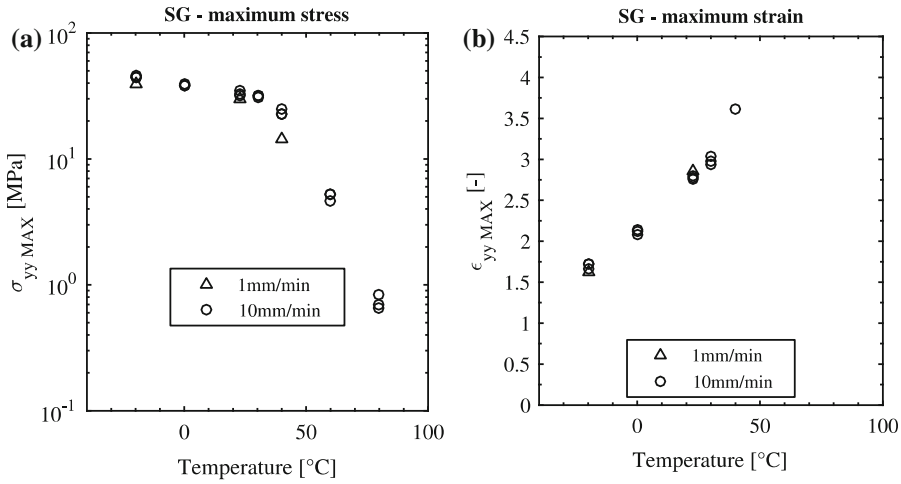

Fig. 20 **a** Effect of temperature variation on SG maximum stress at failure **b** Effect of temperature variation on SG maximum strain at failure

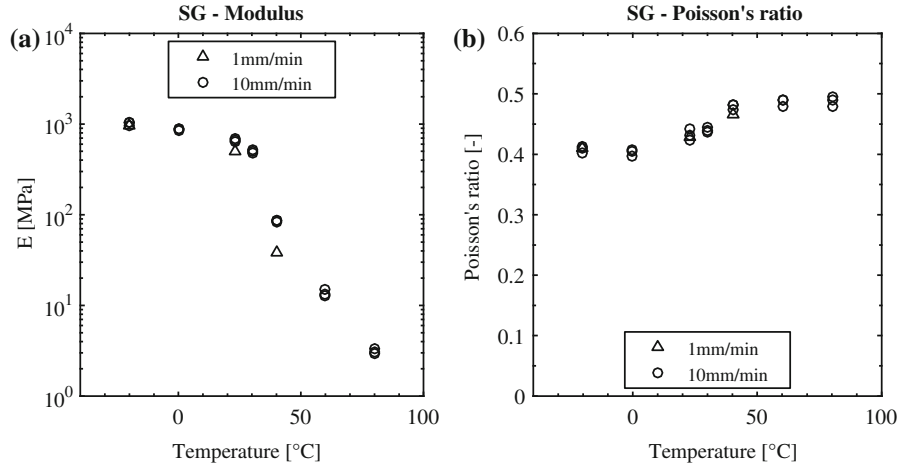

Fig. 21 **a** Effect of temperature variation on SG elastic modulus **b** Effect of temperature variation on SG Poisson's ratio

Finally, the yielding stress is plotted against temperature in Fig. 22. It can be observed that also the yielding stress is temperature and strain rate dependent. It varies from 43 to 0.2 MPa going from −20 to +80 °C. As it happens for the maximum stress and the modulus of elasticity, also the yielding stress shows a significant drop for temperature above 40 °C. When compared to the test at 10mm/min, yielding stress at 23 °C are 15 % larger and 31 % smaller at 100 and 1 mm/min respectively.

In summary, it is found that SG modulus of elasticity, yielding stress and maximum stress at failure show the following similar behaviour. Going from −20 to +80 °C there is an initial gradual decrease with the temperature that is then followed by a significant drop when the temperature exceeds 40 °C. When plotted against temperature, this behaviour exhibits the form of an inverse hyperbolic tangent behaviour. Similar behaviour are be observed in (Santarsiero 2015) for the tensile and shear resistance of laminated connections at different temperatures. The strain rate does not change this behaviour but it simply shifts the values downwards.

4.5 Stress–strain curves at constant true strain rates for model input

In the previous sections it is observed that the displacement rate has significant effects on the material properties of SG and TSSA. This means that the

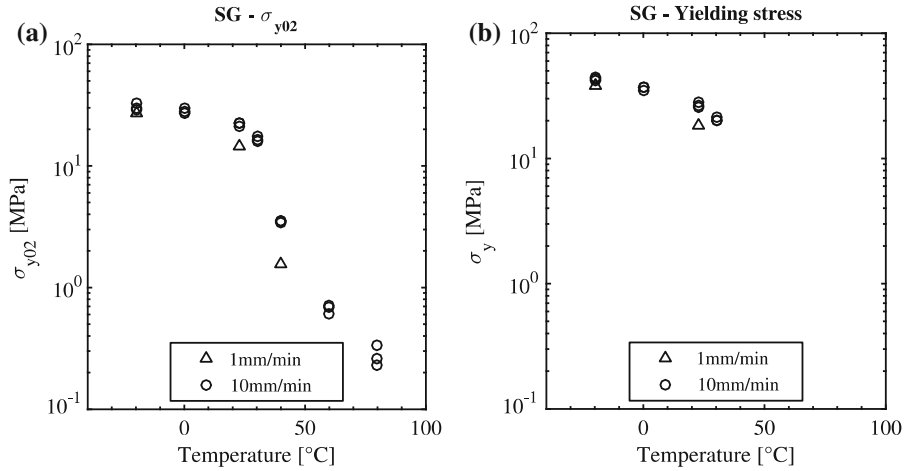

Fig. 22 **a** Effect of temperature variation on SG yielding stress using 0.2 % definition **b** Effect of temperature variation on SG yielding stress

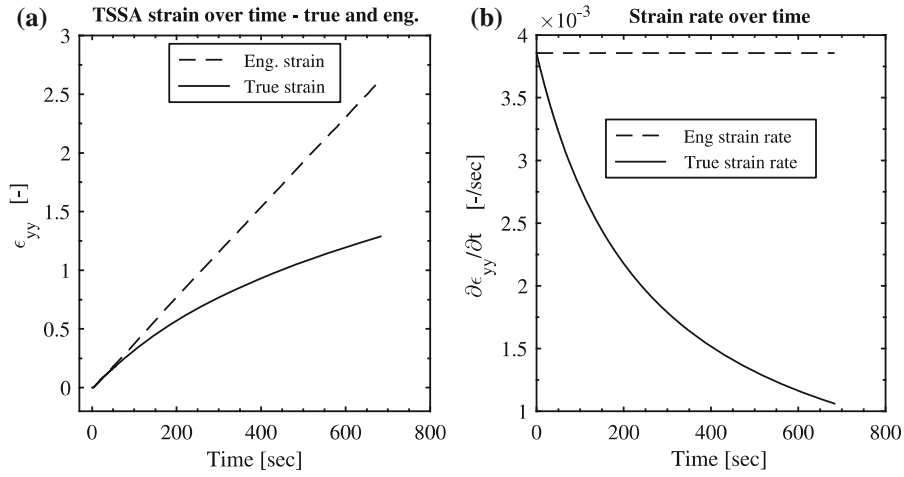

Fig. 23 **a** Engineering and true strain over time **b** Engineering and true strain rate over time

material behaviour depends on the applied strain rate. It follows that, for modelling purposes, stress–strain curves should be associated with the corresponding strain rates. Strain rate is defined as the first derivate of the applied strain over time (see Eqs. (6) and (7), where t is the time variable).

$$\varepsilon_{eng}(t) = \dot{\varepsilon}_{eng}(t) \cdot t \tag{6}$$

$$\frac{\partial \varepsilon_{eng}(t)}{\partial t} = \dot{\varepsilon}_{eng} = constant \tag{7}$$

Now, if the engineering strain definition is used, in uniaxial tensile test constant displacement rate corresponds to constant strain rate[7]. However, in case of large deformations, the finite deformation theory and the true strain definitions should be applied. In this case, constant engineering strain rate does not correspond to true constant strain rate over time. This is shown by Eqs. (8) and (9). The latter expresses true strain rate as a function of time and of the engineering strain rate, which in this case is constant over time.

$$\begin{aligned}\varepsilon_{true}(t) &= \dot{\varepsilon}_{true}(t) \cdot t = ln\left(1 + \varepsilon_{engg}(t)\right) \\ &= ln\left(1 + \varepsilon_{engg} \cdot t\right)\end{aligned} \tag{8}$$

$$\frac{\partial \varepsilon_{true}(t)}{\partial t} = \frac{\dot{\varepsilon}_{eng}}{1 + \varepsilon_{eng}(t)} = \frac{\dot{\varepsilon}_{eng}}{1 + \dot{\varepsilon}_{eng} \cdot t} \tag{9}$$

An example of engineering and true strain measured during a test is plotted in Fig. 23a. As expected engineering and true strains deviate at large deformation. Figure 23a shows engineering strain and true strain measured during the test over time. Fig. 23b shows than that in case of large deformation also the true strain rate

[7] This is assumed to be true under the following hypothesis: (i) the specimen does not slide in the grips during the test and therefore there is no change in the constant displacement rate applied the reference length, (ii) uniform strain field along the specimens, i.e. necking phenomena is not occurring and (iii) constant strain rate in the non-parallel region of the specimens.

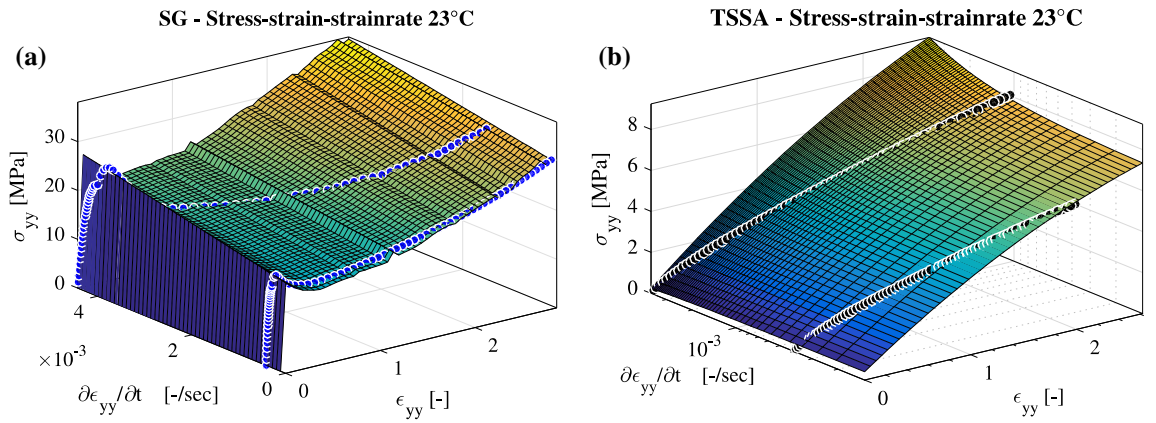

Fig. 24 Three-dimensional graph of stress, strain and strain rate for the determination of stress–strain curves at constant true strain rate and temperature. Matlab non-linear fitting algorithm is used

deviates from the engineering strain rate. More specifically, from the test it is measured that the true strain rate decreases over time, while engineering strain rate is constant over time. This can be physically interpreted considering that when the deformation increases, also the length of the specimens increases. Therefore, considering the finite deformation theory, a constant infinitesimal increment of displacement induces an infinitesimal increase of true strain that reduces over time.

The mechanical material values and the stress–strain curves obtained in this study are used in (Santarsiero 2015) as input for the numerical modelling of laminated connections. In order to implement these material constitutive laws, the stress–strain curves at constant true strain rate are obtained as it follows. The stress–strain curves at variable true strain rate are plotted over a 3D diagram. The three axes of this graph represent stress, strain and strain rate. A 3D surface is then obtained from the plotted data[8] for each temperature. Curves at constant true strain rate are then obtained cutting the surface with stress–strain planes at constant strain rate. Figure 24 shows an example of the three-dimensional stress–strain surface.

5 Conclusions

In this work the mechanical response of TSSA and SG bulk material under uniaxial tensile stress is studied, at different configurations of strain rate and temperature. From the experimental results and data analysis the following conclusions can be drawn.

Firstly, it is observed that the mechanical behaviour of both SG and TSSA are temperature and strain rate dependent. In particular, it is found that maximum stress and strain at failure of TSSA shows a moderate variation with temperature and strain rate. The TSSA modulus of elasticity and Poisson's ratios are instead stable. The effects on the SG material are more pronounced than the TSSA. More in detail, the modulus of elasticity, yielding stress and maximum stress show a significant drop above a temperature of 40 °C. This is because the material approaches and enters the glass transition phase. The SG Poisson's ratio also varies with the temperature, going from 0.41 (at low temperature) to 0.49 (at high temperature).

Secondly, two additional phenomena are observed during the uniaxial tests. For the TSSA material, the so-called whitening phenomenon is observed. The colour of TSSA goes from fully transparent to white when the stress goes above around 5 MPa. For the SG material, it is observed that the strain field distribution is dependent on the temperature. More specifically, at temperature below 40 °C, the material exhibits a non-uniform strain field distribution due to the occurring of a necking phenomenon. The latter consists in a strong strain concentration in the field distribution, occurring when the stress approaches the yielding stress. The necking is consistently inclined at approximately 45° with the uniaxial stress direction, forming the so-called Lüders band. Measurements along the specimens showed that the localized strain propagates over the full specimen

[8] Matlab non-linear fitting algorithm is used.

length, resulting in the cold-drawing phenomenon. It is therefore concluded that local strain measurements are necessary to correctly perform material characterization when the necking phenomenon is occurring.

Finally, it is also shown that engineering and true stress–strain and Poisson's ratio definition exhibits large deviations. This is because both TSSA and SG materials fail at deformation largely over 100 %. It follows that the finite deformation theory should be used for the computation of the stress–strain curves implemented in numerical models.

Acknowledgments The authors would like to thank the Swiss National Science Foundation for founding the present research (Grants 200020_150152 and 200021_134507). In addition, Glas Trösch AG Swisslamex, Kuraray (former Dupont) and Dow Corning are gratefully acknowledged for the material support and specimens preparation. Finally, the COST Action TU0905 "Structural Glass – Novel Design Methods and Next Generation Products" is also acknowledged for facilitating the research network.

Conflict of interest On behalf of all authors, the corresponding author states that there is no conflict of interest.

Appendix A: Uniaxial tensile test results

See Tables 4, 5 and 6.

Table 4 Mechanical material properties of TSSA: values at different temperatures and engineering strain rates

Mooney–Rivlin hyperelastic strain energy potential with coefficients for ABAQUS material model algorithm equal to $D1 = 8.461E-02$, $C10 = 1.1073$, $C01 = 0.1154$

T (°C)	$\dot{d}$ (mm/min)	$\dot{\varepsilon}$ (−/s)	E (MPa)	v (–)	$\sigma_{yy.max}$ (MPa)	$\sigma_{yy.max.true}$ (MPa)	$\varepsilon_{yy.max}$ (–)	$\varepsilon_{yy.max.true}$ (–)
80	1	4E−04	6.79	0.46	5.00	10.91	1.33	0.85
23	1	4E−04	6.23	0.43	6.13	15.89	1.99	1.09
−20	1	4E−04	6.39	0.46	7.52	23.39	2.21	1.17
80	10	4E−03	6.85	0.45	6.12	14.96	1.62	0.96
80	10	4E−03	6.97	0.46	5.91	14.25	1.58	0.95
80	10	4E−03	7.04	0.44	6.15	14.83	1.59	0.95
23	10	4E−03	6.48	0.44	7.81	20.86	2.61	1.28
23	10	4E−03	6.42	0.44	7.76	21.26	2.52	1.26
23	10	4E−03	6.44	0.42	8.03	21.81	2.62	1.29
−20	10	4E−03	6.42	0.44	9.90	32.66	3.02	1.39
−20	10	4E−03	6.67	0.42	9.96	33.11	2.86	1.35
−20	10	4E−03	6.63	0.44	8.87	29.32	2.58	1.27
23	100	4E−02	7.1	0.46	8.03	22.82	2.14	1.13

Table 5 Mechanical material properties of SG: values at different temperatures and engineering strain rates

T (°C)	$\dot{d}$ (mm/min)	$\dot{\varepsilon}$ (−/s)	E (MPa)	v (–)	$\sigma_{yy.max}$ (MPa)	$\sigma_{yy.max.true}$ (MPa)	$\varepsilon_{yy.max}$ (–)	$\varepsilon_{yy.max.true}$ (–)
40	1	4.E−04	37.65	0.47	14.21	42.82	n/a	n/a
23	1	4.E−04	505.52	0.43	29.88	120.16	2.86	1.35
−20	1	4.E−04	966.19	0.41	39.49	99.39	1.62	0.96
80	10	4.E−03	2.96	0.48	0.66	2.65	n/a	n/a
80	10	4.E−03	3.09	0.49	0.70	3.08	n/a	n/a
80	10	4.E−03	3.35	0.49	0.83	3.50	n/a	n/a
60	10	4.E−03	12.58	0.48	5.16	19.31	n/a	n/a
60	10	4.E−03	13.14	0.49	4.61	17.77	n/a	n/a
60	10	4.E−03	14.86	0.49	5.22	18.96	n/a	n/a
40	10	4.E−03	86.22	0.48	22.90	84.77	n/a	n/a
40	10	4.E−03	86.29	0.48	22.70	82.50	n/a	n/a
40	10	4.E−03	84.90	0.48	25.18	105.54	3.61	1.53
30	10	4.E−03	479.46	0.44	31.40	114.70	2.97	1.38
30	10	4.E−03	520.65	0.45	31.68	120.38	2.93	1.37

Table 5 continued

T (°C)	$\dot{d}$ (mm/min)	$\dot{\varepsilon}$ (−/s)	E (MPa)	υ (–)	$\sigma_{yy.max}$ (MPa)	$\sigma_{yy.max.true}$ (MPa)	$\varepsilon_{yy.max}$ (–)	$\varepsilon_{yy.max.true}$ (–)
30	10	4.E−03	496.78	0.44	30.65	118.95	3.03	1.39
23	10	4.E−03	700.67	0.42	34.35	120.74	2.80	1.33
23	10	4.E−03	659.92	0.44	32.22	115.78	2.75	1.32
23	10	4.E−03	650.05	0.43	32.34	115.50	2.77	1.33
0	10	4.E−03	868.20	0.41	38.25	109.17	2.09	1.13
0	10	4.E−03	846.96	0.40	37.80	111.70	2.15	1.15
0	10	4.E−03	877.16	0.40	38.94	120.57	2.13	1.14
−20	10	4.E−03	961.75	0.40	44.22	115.40	1.72	1.00
−20	10	4.E−03	1036.00	0.41	44.22	176.37	1.67	0.98
−20	10	4.E−03	1040.00	0.41	46.43	210.60	1.72	1.00
23	100	4.E−02	700.96	0.43	34.47	136.54	3.00	1.39

n/a Stroke machine capacity is reached for temperature above 40 °C. Only one specimen at 40 °C failed before stroke capacity

Table 6 Mechanical material properties of SG: values of yielding stress at different temperatures and engineering strain rates

T (°C)	$\dot{d}$ (mm/min)	$\dot{\varepsilon}$ (−/s)	σ_y (MPa)	σ_{y02} (MPa)
40	1	4.E−04	n/a	2.77
23	1	4.E−04	19.62	19.00
−20	1	4.E−04	42.77	35.82
80	10	4.E−03	n/a	0.69
80	10	4.E−03	n/a	0.61
80	10	4.E−03	n/a	0.61
60	10	4.E−03	n/a	2.06
60	10	4.E−03	n/a	2.27
60	10	4.E−03	n/a	2.22
40	10	4.E−03	n/a	5.27
40	10	4.E−03	n/a	5.30
40	10	4.E−03	n/a	5.17
30	10	4.E−03	21.65	19.85
30	10	4.E−03	23.19	21.87
30	10	4.E−03	22.01	20.64
23	10	4.E−03	29.75	28.50
23	10	4.E−03	28.52	27.11
23	10	4.E−03	27.72	26.73
0	10	4.E−03	40.22	35.69
0	10	4.E−03	37.61	34.69
0	10	4.E−03	40.17	36.76
−20	10	4.E−03	47.60	39.40
−20	10	4.E−03	48.79	39.96
−20	10	4.E−03	48.65	42.81
23	100	4.E−02	32.9	28.43

n/a no yield can be observed

References

American Society for Testing and Materials.: ASTM D412-06a Standard Test Methods for Vulcanized Rubber and Thermoplastic Elastomers-Tension. Annual Book of ASTM Standards, p. i (2008)

Belis, J., et al.: Failure mechanisms and residual capacity of annealed glass/SGP laminated beams at room temperature. Eng. Fail. Anal. **16**(6), 1866–1875 (2009). doi:10.1016/j.engfailanal.2008.09.023

Bennison, S.J., et al.: Laminated glass for blast mitigation: role of interlayer properties. In: Glass Processing Days (2005)

Biolzi, L., Cattaneo, S., Rosati, G.: Progressive damage and fracture of laminated glass beams. Constr. Build. Mater. **24**(4), 577–584 (2010). doi:10.1016/j.conbuildmat.2009.09.007

Calgeer, L.: Structural design of glass façade components: comparison of different connection typologies. Master Thesis Dissertation, École Polytechnique Fédérale De Lausanne: EPFL (2015)

CEN-European Committee for Standardisation.: EN 10088-2—Stainless steel—Part 2: Technical delivery conditions for sheet/plate and strip of corrosion resisting steels for general purposes

CEN-European Committee for Standardisation.: EN ISO 527-2 Determination of tensile properties of plastic (1996)

da Silva, L.F.M., et al.: Testing Adhesive Joints. Wiley-VCH, Weinheim (2012)

Decourcelle, R., Nugue, J.C. Levasseur, F.: Mechanical participation of interlayer on laminated glass for building applications. In: Glass Performance Days, pp. 718–721 (2009)

Ehrenstein, G.W.: Polymeric Materials: Structure, Properties, Applications. Hanser, Munich (2001)

Eisenberg, A., Rinaudo, M.: Polyelectrolytes and ionomers. Polym. Bull. **24**, 671 (1990)

European Organisation for Technical Approvals.: ETAG 002 - Guideline for European Technical approval for Structural Sealant Glazing Systems (SSGS) Part 1 : Supported and unsupported system (2001)

François, D., Pineau, A., Zaoui, A.: Mechanical Behaviour of Materials. Fracture Mechanics and Damage, vol. 2. Springer, New York (2013)
Gottstein, G.: Physical Foundations of Materials Science. Springer, Berlin (2004)
Hagl, A., Wolf, A.T., Sitte, S.: Investigation of stress-whitening in transparent structural silicon adhesive. In: Challenging Glass, vol. 3 (2012)
International Organization for Standardization.: ISO 37 - Rubber, vulcanized or thermoplastic—determination of tensile stress-strain properties (2011)
Kuntsche, J., Schneider, J.: Mechanical behaviour of polymer interlayers in explosion resistant glazing. In: Challenging Glass 4 & COST Action TU0905 Final Conference, pp. 447–454 (2014)
Lenk, P., Lancaster, F.: Connections in structural glass. In: Glass Performance Days (2013)
Macknight, W.J., Earnest, J.: The structure and properties of ionomers. J. Polym. Sci.: Macromol. Rev. **19**, 41–122 (1981). doi:10.1002/pol.1981.230160102
Meissner, M., Sackmann, V.: On the effect of artificial weathering on the shear bond and the tear strength of two different interlayers of laminated glass. In: ISAAG (2006)
O'Callaghan, J.: Adventures with structural glass. In: Glass Performance Days (2012)
O'Callaghan, J., Coult, G.: An all glass cube in New York City. In: Glass Performance Days (2007)
Pelleg, J.: Mechanical Properties of Materials. Springer, New York (2008)
Peters, S., et al.: Ganzglastreppe mit transparenten SGP-Klebeverbindungen - Konstruktion und statische Berechnung. Stahlbau **76**(3), 151–156 (2007). doi:10.1002/stab.200710017
Puller, K.: Untersuchung des Tragverhaltens von in die Zwischenschicht von Verbundglas integrierten Lasteinleitungselementen. Thesis Dissertation, University of Stuttgart (2012)
Puller, K., Denonville, J., Sobek, W.: An innovative glass connection technique using an ionomer interlayer. In: Glass Performance Days, Tampere (2011)
Raghava, R.S., Caddell, R.M.: A macroscopic yield criterion for crystalline polymers. Int. J. Mech. Sci. **15**(12), 967–974 (1973). doi:10.1016/0020-7403(73)90106-9
Roylance, D.: Mechanics of Materials. Wiley, New York (1996)
Santarsiero, M.: Laminated connections for structural glass applications. Thesis Dissertation, École Polytechnique Fédérale De Lausanne - EPFL (2015)
Schneider, J. et al.: Tensile properties of different polymer interlayers under high strain rates. In: Engineered Transparency (2012)
Sitte, S., et al.: Preliminary evaluation of the mechanical properties and durability of transparent structural silicone adhesive (TSSA) for point fixing in glazing. J. ASTM Int. **8**(10), 1–27 (2011). doi:10.1520/JAI104084
Stelzer, I.: High performance laminated glass. In: Challenging Glass, vol. 2, Delft (2010)
Varley, R.: Ionomers as self healing polymers. In: van der Zwaag, S. (ed.) Self Healing Materials. An Alternative Approach to 20 Centuries of Materials Science, pp. 95–114. Springer, New York (2007)